Mechanism of formation Co-Ru nanoalloys: the key role of Ru on the reduction pathway of Co

Brandon Azeredo,[a,b] Tayssir Ben Ghzaiel,[a] Ning Huang,[a] Sophie Nowak,[a] Jennifer Peron,[a] Marion Giraud,[a] Jeyadevan Balachandran,[c] Olivier Taché,[d] Laurent Barthe,[e] Jean-Yves Piquemal,*[a] Valérie Briois,[e] Lorette Sicard*[a]

[a]Université Paris Cité, CNRS, ITODYS, F-75013 Paris, France
[b]Université de Toulouse, Laboratoire de Physique et Chimie des Nano-Objets, UMR 5215 INSA, CNRS, UPS, 135 Avenue de Rangueil, F-31077 Toulouse, cedex 4, France
[c]Graduate School of Environmental Studies, Tohoku University, Sendai 980-8579, Japan
[d]Laboratoire Interdisciplinaire sur l'Organisation Nanométrique et Supramoléculaire, Université Paris Saclay, NIMBE UMR 3685 CEA-CNRS 91191 Gif sur Yvette, France.
[e]Synchrotron SOLEIL, L'Orme des Merisiers, Départementale 128, 91190 Saint-Aubin, France.

*Corresponding authors: lorette.sicard@u-paris.fr, jean-yves.piquemal@u-paris.fr

Supplementary Information

Content

S1. UV-visible spectroscopy

The spectra of octan-1-ol and of acetylacetonate complexes of Co(II), Ru(III) and Na(I) in this solvent are given in Figure S1. These spectra were recorded at a lower concentration (10 times lower, *i.e.* 1.63 mM) than that used for the synthesis. Attributions of the peaks are gathered in Table S1.

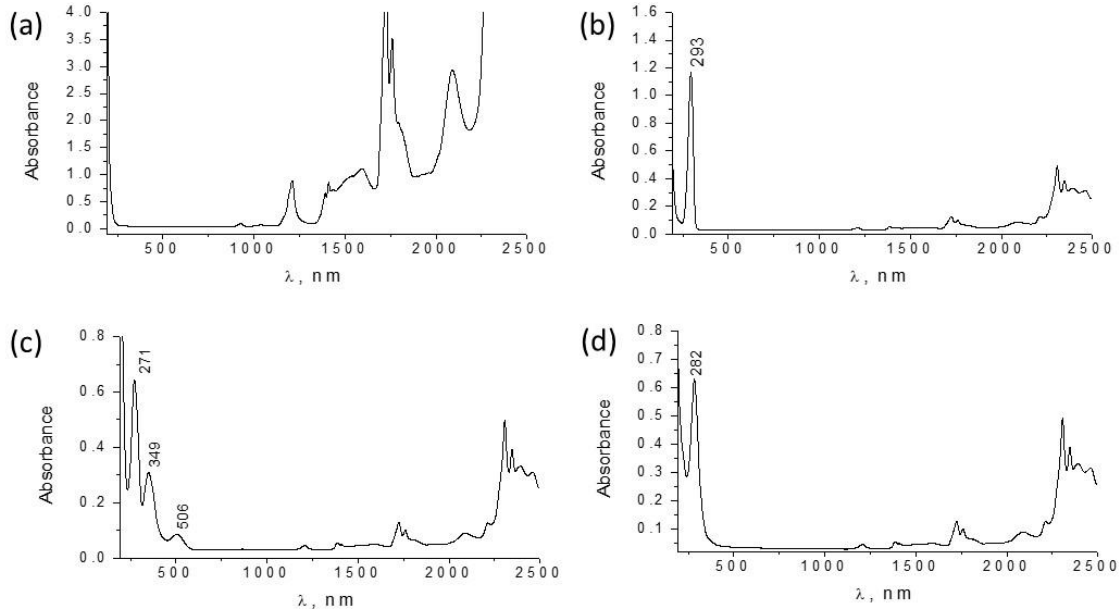

Figure S1. UV-visible spectra of octan-1-ol (a), and acetylacetonate complexes in octan-1-ol: Na(acac), 3.26 mM (b), $Ru(acac)_3$, 1.63 mM (c), $Co(acac)_2$, 1.63 mM (d). The cuvette path length was l = 0.2 mm except for (a), where it was l = 1 cm.

Table S1. Attributions and molar absorption coefficients for the electronic transitions observed for Na(acac), $Co^{II}(acac)_2$ et $Ru^{III}(acac)_3$ solutions in octan-1-ol.

Compound	**λ, nm**	**Attribution**	**ε, L·mol^{-1}·cm^{-1}**
Na(acac)	293	acac π → acac π*	17950
$Co^{II}(acac)_2$	282	acac π → acac π*	19330
$Ru^{III}(acac)_3$	271	acac π → acac π*	19000
	349	Charge transfer	7900
	506	Charge transfer	1590

The UV-vis-NIR spectrum of Na(acac) in octan-1-ol (Figure S1.b) displays a well-defined peak at *ca.* 293 nm which is attributed to a π→π* transition.[1,2] Other peaks are visible in the near infrared: they correspond to vibrations modes of octan-1-ol (see Figure S1.a).

The spectrum of $Ru(acac)_3$ is similar to that reported in the literature [2] with three maxima at 271, 349 and 506 nm (Figure S1.c). The absorption coefficients deduced from the Beer Lambert law are given in Table S1. They are all higher than 1000 $L \cdot mol^{-1} \cdot cm^{-1}$; hence they cannot correspond to d-d transitions. The first peak at 271 nm was attributed to a $\pi \rightarrow \pi^*$ transition of the acac ligand. The slight shift compared to Na(acac) is probably due to its coordination to Ru(III). The two other peaks at 349 and 506 nm can be assigned to charge transfer transitions.

The spectrum of $Co(acac)_2$ is given in Figure S1.d. The main peaks are those corresponding to octan-1-ol in the near-IR region and an intense peak at 282 nm, which was attributed to the $\pi \rightarrow \pi^*$ transition of acac coordinated to Co(II). The value of the absorption coefficient, close to the previously calculated ones, supports this attribution.

S2. XAS experiments

S2.1. Cell designed for *in situ* analyses and set-up

A specific cell was designed for the *in situ* XAS experiments to meet our needs. A scheme and a photo of this cell are given in Figure S2.

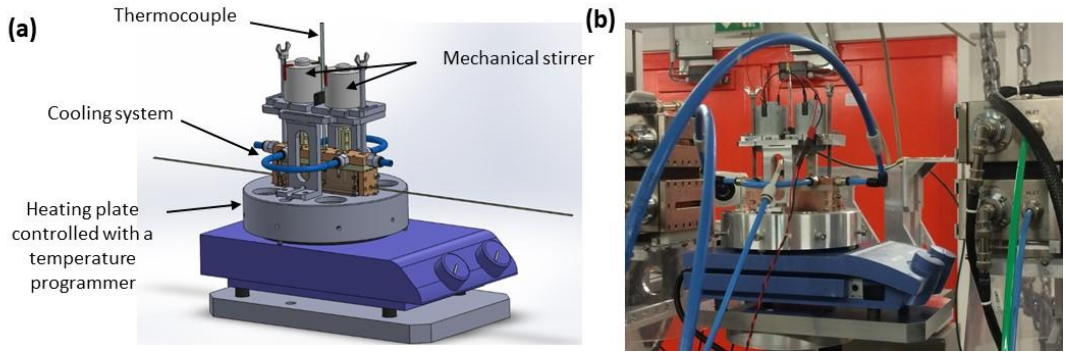

Figure S2. (a) Scheme of the cell designed for the *in situ* study of the kinetics of reduction of Ru(III) and Co(II) ions and (b) photo of the cell on the ROCK beamline (SOLEIL Synchrotron facility).

The cell is composed of two parts. The external part of the cell is in copper, while the internal part is in polyetheretherketone (PEEK). This latter is 0.6 cm in width and 8 cm in length, with X-ray windows obtained in the width direction by thinning PEEK down to a thickness of 200 μm for a better transmission of X-rays at the Co K edge (≈ 8 keV). No thinning is required in the length direction, thanks to the higher penetrating depth of X-rays at the Ru K edge energy (≈ 22 keV). In this optical path the walls are 8 mm thick. The copper block has small apertures at the place of the X-rays windows in the

PEEK cell in order to allow the transmission of X-rays towards the ionization chamber measuring the photon flux transmitted by the solution. The cell was used with the optical path of 8 cm to record spectra at the Ru-K edge whereas it was placed perpendicularly to obtain an optical path of 0.6 cm at the Co-K edge. $Co(acac)_2$ and $Ru(acac)_3$ were previously dissolved in octan-1-ol with a global metal concentration of 16.3 mM and a ratio depending on the alloy studied. 7 mL of this solution were introduced in the PEEK cell. Two rotating overhead stirrer paddles in PEEK allowed mechanical stirring of the solution. The cell was closed but not hermetically to avoid over-pressure because some gas is released during the reaction. Argon was flushed into the cell via a hole before heating.

The copper external part of the cell was placed on a heating plate linked to a temperature regulator, allowing heating the reactive solution to the boiling point. The temperature was increased stepwise with an average speed of 5 °C.min^{-1}. A typical profile is given in Figure S3. The non-linear ramp and the occurrence of overshootings explain that the evolutions deduced from XAS experiments are not smooth but the general species evolution can be relied on, as attested by the fact that they are the same than that deduced from UV-visible spectroscopy and as the evolution of the species does not show any disruption. A cooling system limited the evaporation of the solvent but did not prevent it completely. Due to the loss of solution coupled to the presence of bubbles at the boiling point, we could not afford the monitoring during the isothermal stage at 180°C and the results presented here concern only the heating period.

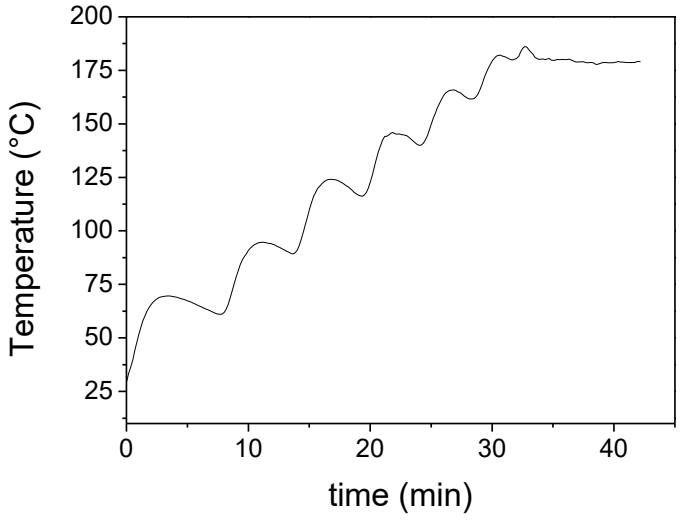

Figure S3. Heating profile recorded during the XAS experiments at the Ru-K-edge of a solution of $Ru(acac)_3$ in octan-1-ol.

S2.2. X-ray Absorption Spectroscopy at the Ru K-edge

Figure S4 displays the evolution of the XAS spectra at the Ru K-edge for all the compositions during heating. Figures S5 and S6 give, respectively, the evolution of the energy for a normalized absorbance

of 0.3 and of the white line intensity as a function of the temperature, deduced from the data of Figure S5. Their rapid decrease from *ca.* 160 - 170 °C for all the compositions can be accounted for the reduction of Ru(III) species. It is to note that the non-monotonous decrease is due to the heating profile (Figure S3) which shows some overshootings followed by small decreases in temperature. The white line intensity and shift energy values never decrease during the experiment, showing that the reduction is not reversible.

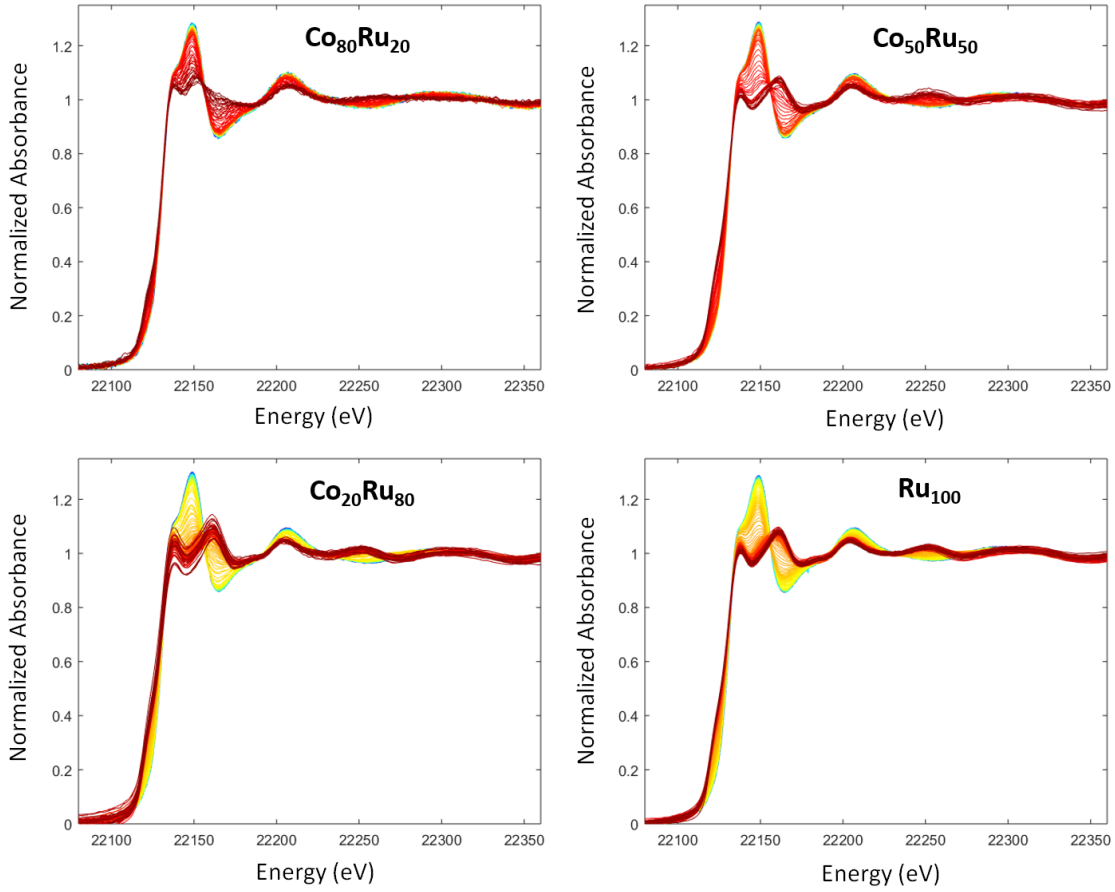

Figure S4. Normalized XAS spectra at Ru K-edge obtained during heating the reactive solutions of Co_xRu_{100-x}, x = 80, 50, 20, 0. The colour of the spectra shifts from blue at room temperature to red at the end of the experiment (stage at the boiling temperature).

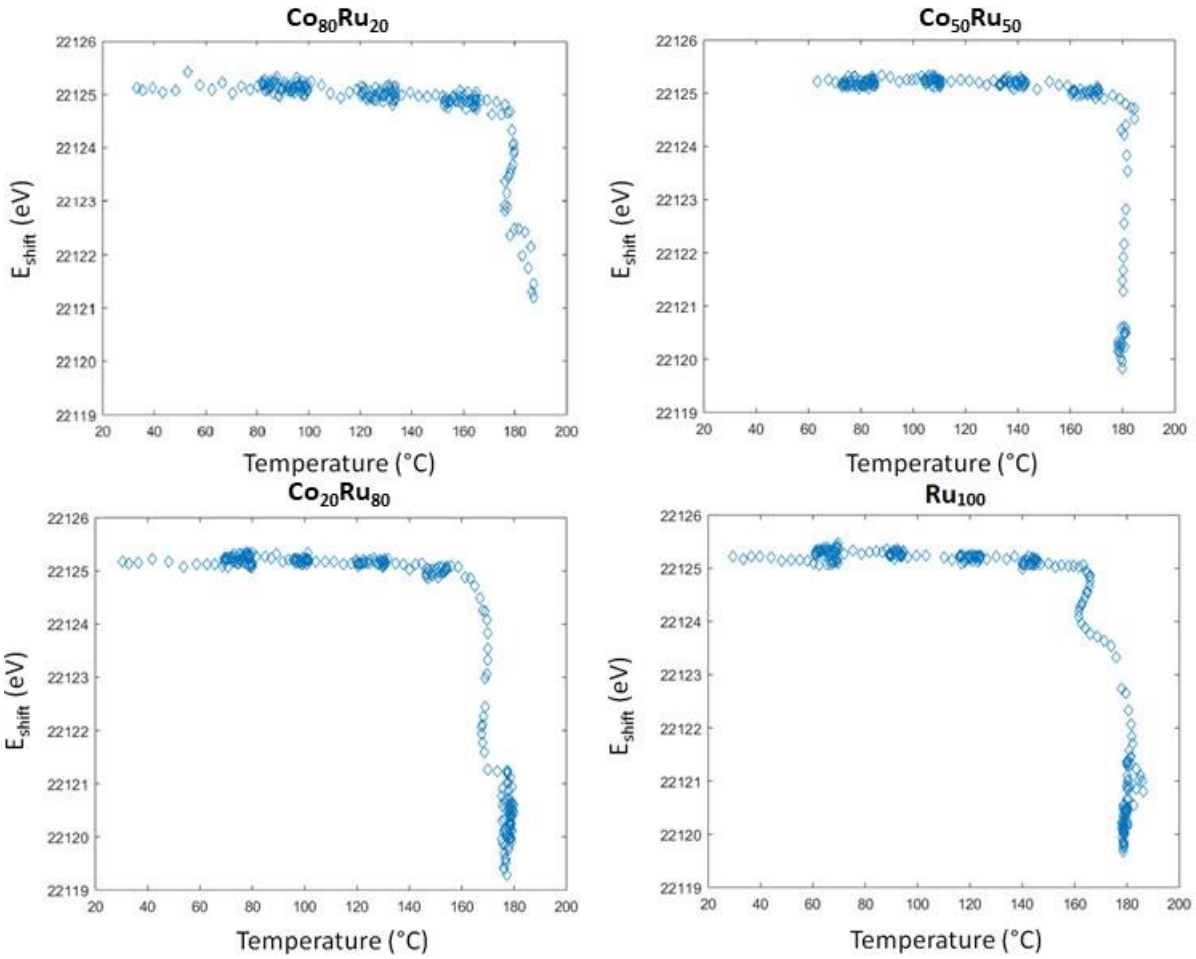

Figure S5. Energy measured at a normalized absorbance of 0.3 during heating of the precursor solutions.

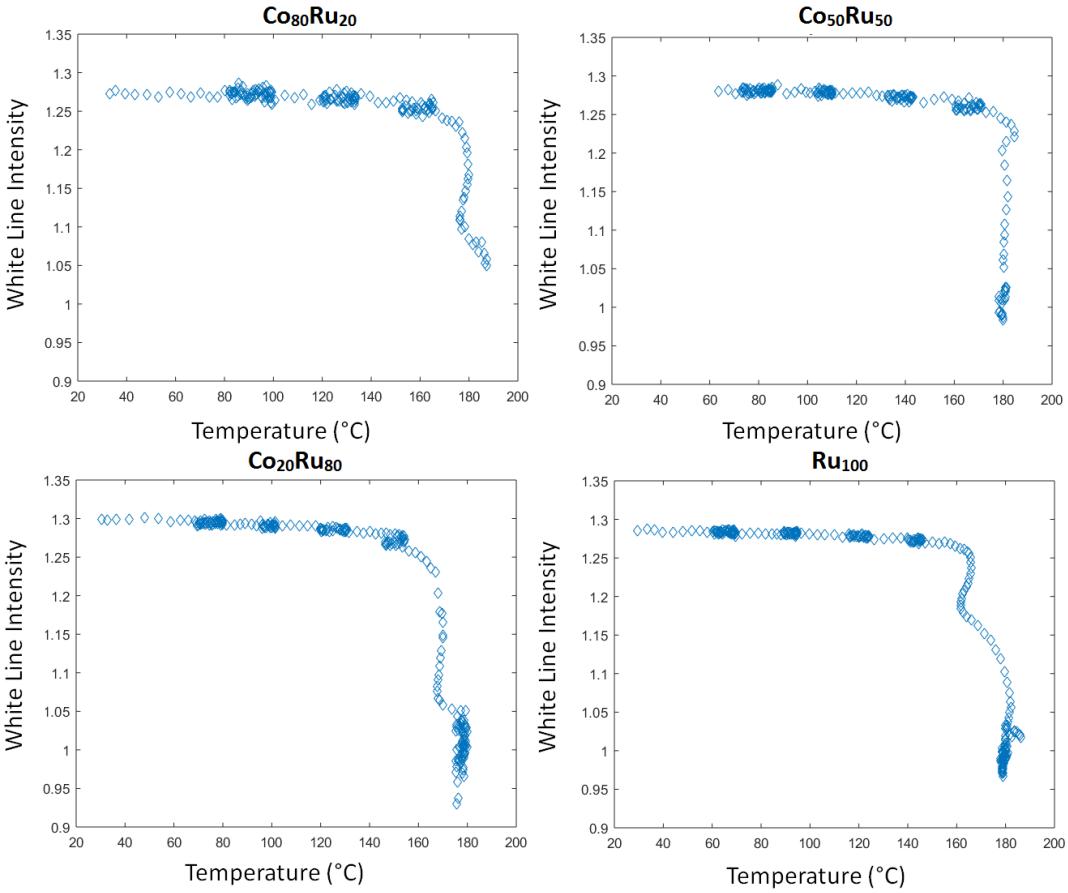

Figure S6. White line intensity evolution during heating the precursor solutions of different compositions.

Principal Component Analysis (PCA) was carried out for each composition. The Scree plot[4] which displays the eigenvalues associated to each principal component (PC) in descending order *versus* the first 20 PC was used to determine the number of species involved in the reaction mixture. Only 2 species were necessary to account for the reduction of Ru cations in the different precursor solutions.

The treatment of the four sets of data gave a common spectrum characteristic of Ru(III) before heating for all compositions. However, the spectra obtained at the end of the heating step were slightly different suggesting that the reduction rate is not at the same level for the different solutions, which is normal as the stage duration was not exactly the same for all the compositions. The isolation of pure species for incomplete 1-stepped reaction can be limited by the reaction rate. To overcome this issue, the experience matrices of the 4 compositions were gathered and treated in a Column-Wise matrix Augmentation (CWA) strategy. For this simultaneous data treatment, it was assumed that the two spectra explaining the variance of the four CWA data set were identical. Constraints used for the minimization were non-negativity of concentrations and absorbance in the spectra, closure of concentrations and unimodality of concentration profile for each composition. The spectra resulting

from the minimization by MCR-ALS are presented in Figure S7 and the quality factor of the analysis in Table S2. The MCR-ALS spectrum of the initial species superimpose with that of the initial solution. That of the MCR-ALS spectrum of the final species differs slightly from the spectrum recorded *in situ* at the end of the experiments. It is obviously an approximation since the different species should be NPs with different proportions of Co and Ru according to the solution composition. Nevertheless, the validity of the approach is further validated by the fact that, irrespective of the composition, a satisfactory reconstruction of the experimental data corresponding to the end of the reactions has been achieved by combination of the two spectra obtained by this method as displayed in Figure S8.

Table S2. Quality factor of the MCR-ALS analysis of the Ru K edge XAS data (between 21855 – 22425 eV)

MCR-ALS Quality Indicator as defined in Ref [5]	Value
Standard Deviation of residual *vs*. experimental data	0.005181
Fitting error (lack of fit) in (%) of experimental data	0.68743
Percentage of variance explained at the optimum	99.9953

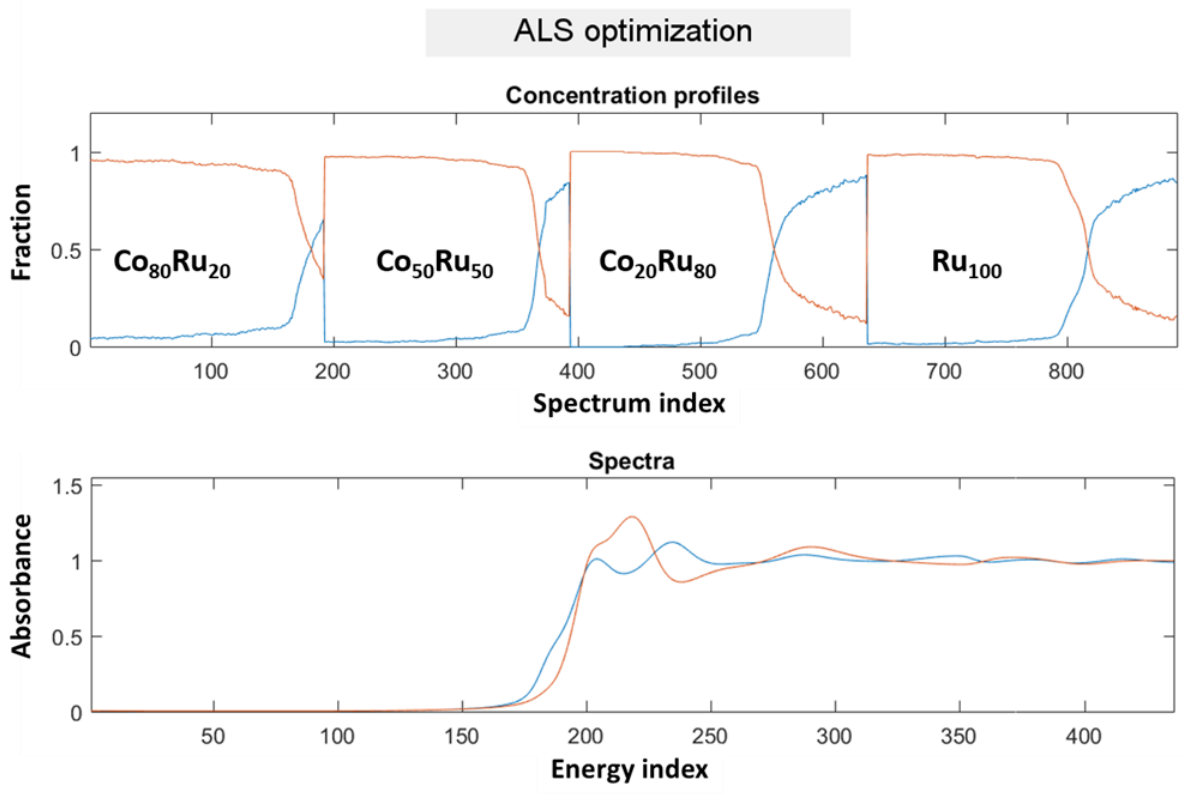

Figure S7. Results of the CWA minimization by MCR-ALS of the matrix obtained by the concatenation of the XAS data recorded at the Ru Kedge for the $Co_{80}Ru_{20}$ composition (from spectrum index #1 to spectrum index #192), the $Co_{50}Ru_{50}$ composition (from spectrum index #193 to spectrum index #394), the $Co_{20}Ru_{80}$ composition (from spectrum index #395 to spectrum index #637) and the Ru_{100} composition (from spectrum index #638 to spectrum index #890). The red and blue curves are presenting the fraction (top) and MCR-ALS spectrum (bottom) of the initial and final species, respectively.

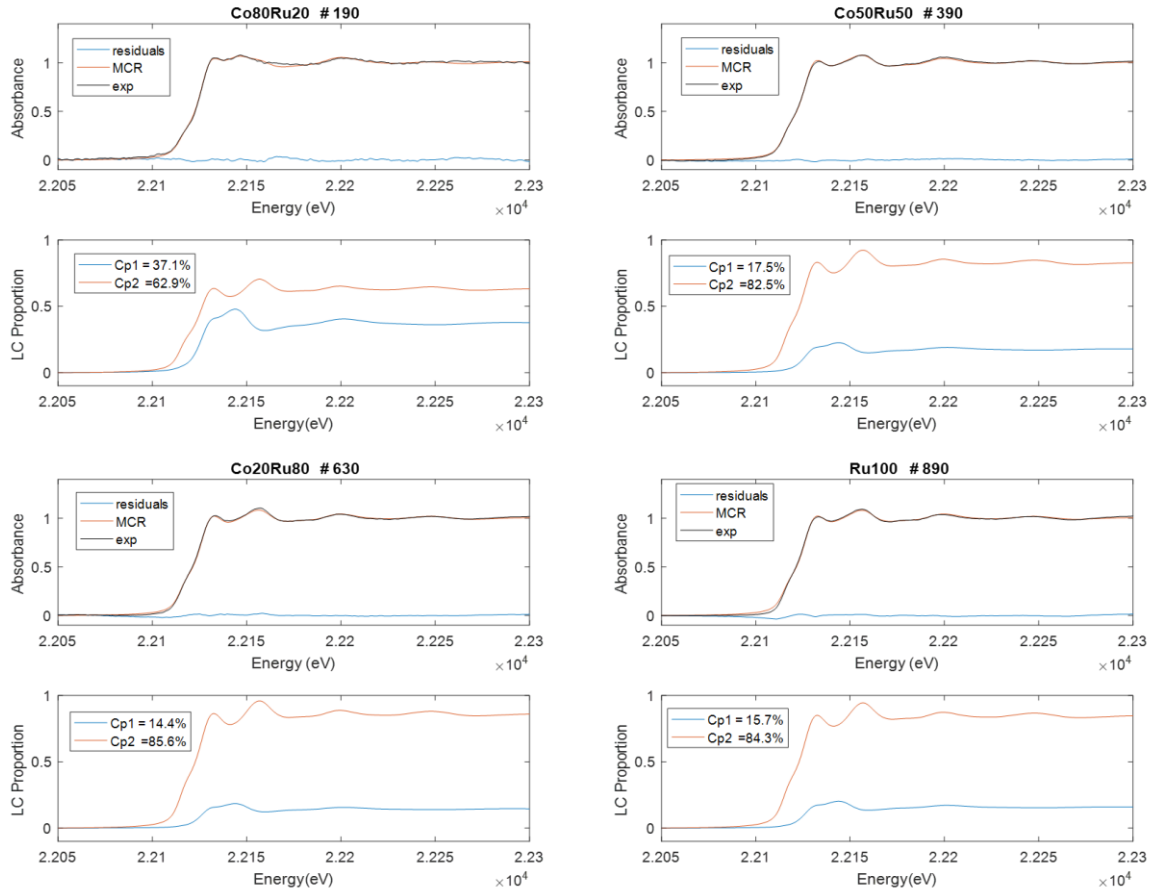

Figure S8. Comparison of the Ru K edge experimental spectrum (black line) obtained at the end of the kinetics for the four sample compositions with the MCR-ALS rebuilt spectrum (red line) and corresponding residuals (blue line) corresponding to the difference between the experimental spectrum and rebuilt one. The weighted spectral contribution of each component (Cp1 and Cp2) used to rebuild each spectrum is also reported. The residual factor for reconstruction of each spectrum was 1.45 % for $Co_{80}Ru_{20}$, 1.47 % for $Co_{50}Ru_{50}$, 1.12 % for $Co_{20}Ru_{80}$ and 1.40 % for Ru_{100}.

The data and the fits of the k^2 weighted Ru K EXAFS and the corresponding EXAFS Fourier transformed (FT) moduli of the Ru and $Co_{80}Ru_{20}$ NPs are given in Figure S9. The FT recorded for the $Co_{80}Ru_{20}$ powder displays, besides the Ru-Ru bond contribution seen at *ca.* 2.4 Å, a second contribution at about 2.1 Å corresponding to Ru-Co bonds. At R lower than 2.0 Å, the contribution is due to Ru-O bonds. It is noteworthy that the peak position in the EXAFS Fourier transformed moduli does not correspond to the crystallographic distance between the absorbing atom and its neighboring atoms as they do in a Radial Distribution Function. The peak positions are shorter by ≈0.3-0.4 Å than the crystallographic distances, these ones are recovered only after a Least Squares minimization procedure. The fitted parameters are given in the main text of the article.

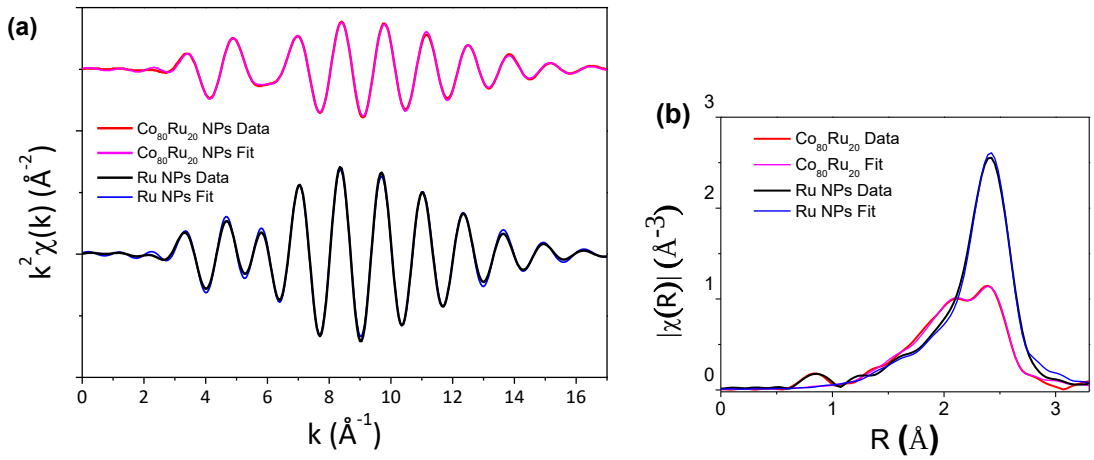

Figure S9. a) Data and fit of a) k^2 weighted Ru K EXAFS and b) corresponding EXAFS Fourier transformed moduli for both Ru and $Co_{80}Ru_{20}$ NPs. The fits were made between R= 1 and 3 Å ; from k = 4 to 16 with dk = 2 (Kaiser Bessel).

S2.3. X-ray Absorption Spectroscopy at the Co K-edge

XAS spectra at the Co K-edge were also recorded during heating solutions of $Co(acac)_2$ or mixtures of $Co(acac)_2$ and $Ru(acac)_3$ in octan-1-ol. The obtained spectra are given in Figure S10.

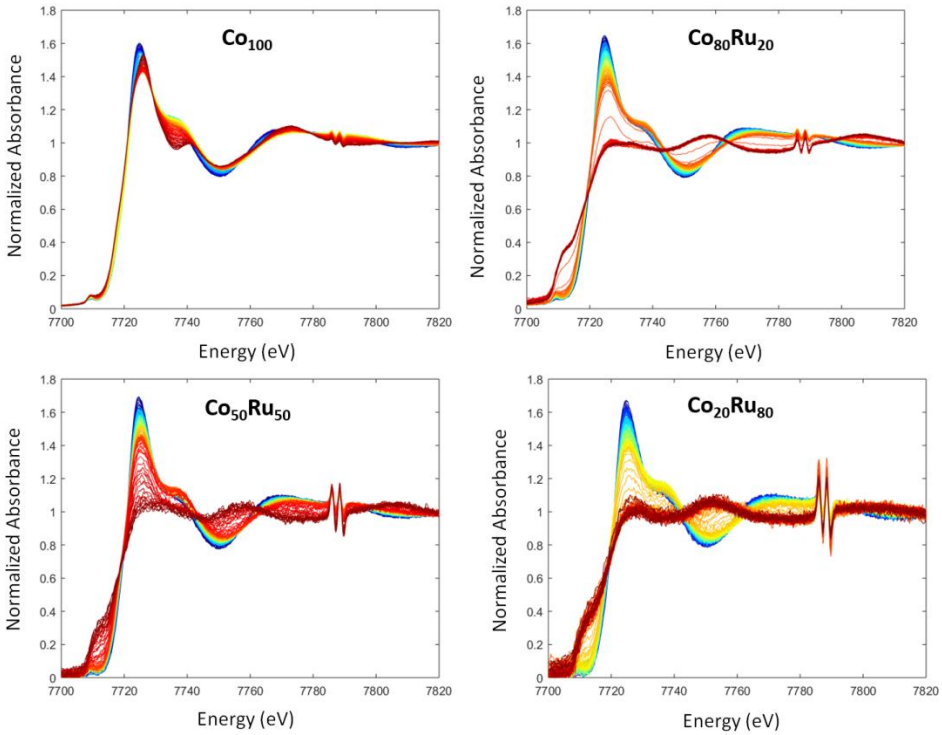

Figure S10. Normalized spectra at the Co K-edge obtained when heating the precursor solutions of Co, $Co_{80}Ru_{20}$, $Co_{50}Ru_{50}$, $Co_{20}Ru_{80}$ NPs (the colour evolves from blue at the beginning of the experiment to red at the end). The feature located near 7790 eV is a monochromator glitch which arises from the fact that the primary

diffracted beam by the monochromator undergoes a second diffraction from a different set of crystal atomic plane inducing an intensity loss of the X-rays going to the sample. Smaller is the cobalt composition in the sample, higher will appear the glitch on the data.

The evolutions of the energy with temperature for a normalized absorbance of 0.3 and of the white line intensity are given in Figures S11 and S12, respectively. There is a marked difference between the solution containing Co cations only and those containing also Ru cations. In the first case, only a slight decrease of the white line intensity together with a slight shift of its energy position (less than 2 eV) are observed but no significant variation in energy of the rising edge occurs. For the Ru-containing solutions, the intensity of the white line decreases much more and the shoulder in the rising edge is much more marked. For those solutions, a 2-stepped evolution is observed. From RT to about 160°C, only the white line significantly decreases in intensity from *ca.* 1.6 to 1.4 with no marked change of the rising edge position, whereas an abrupt shift of edge position and of the white line intensity occurs above 160°C to the values characteristic of metallic cobalt.

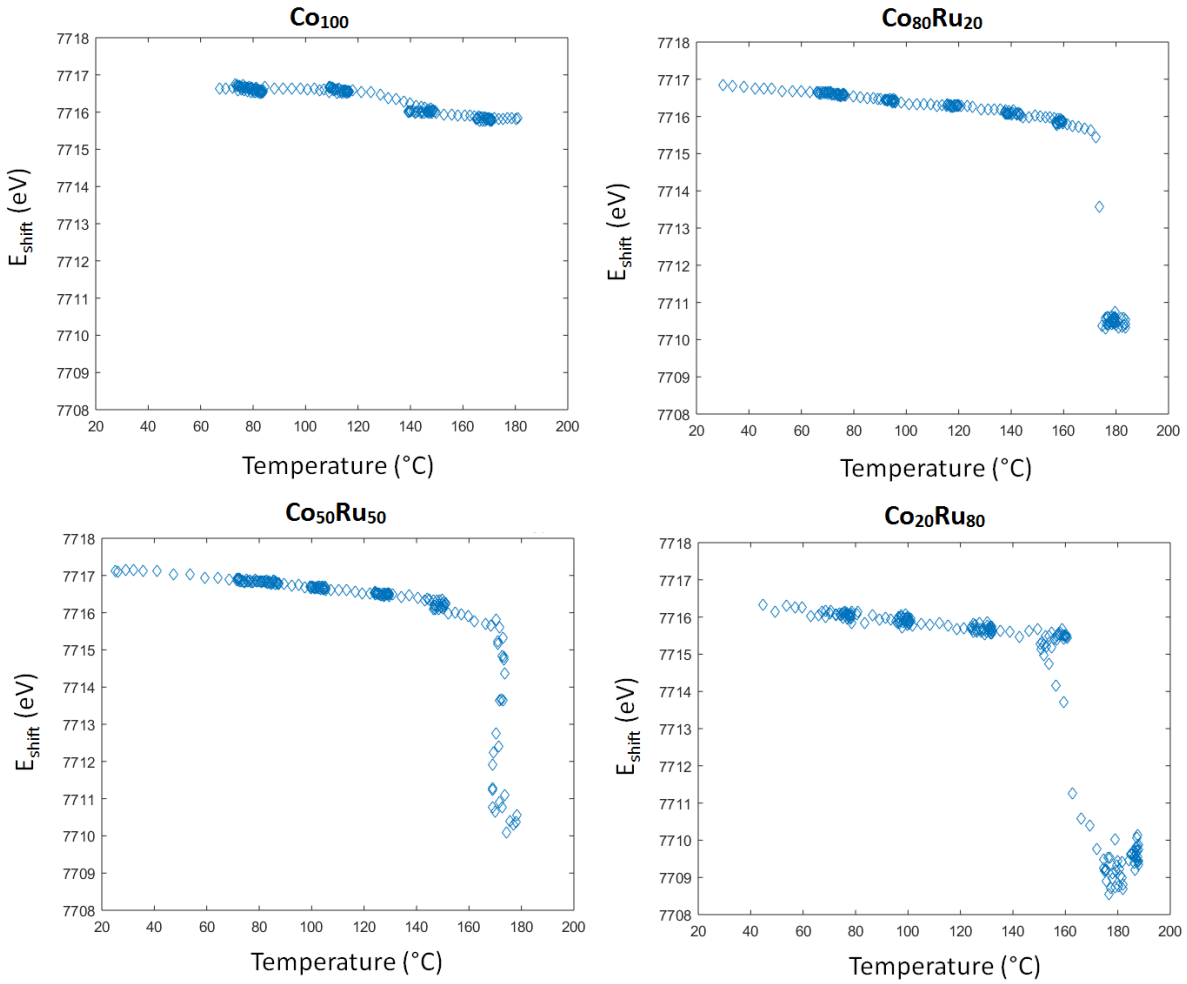

Figure S12. Shift in energy of the edge at 0.3 normalized absorbance during heating the precursor solutions.

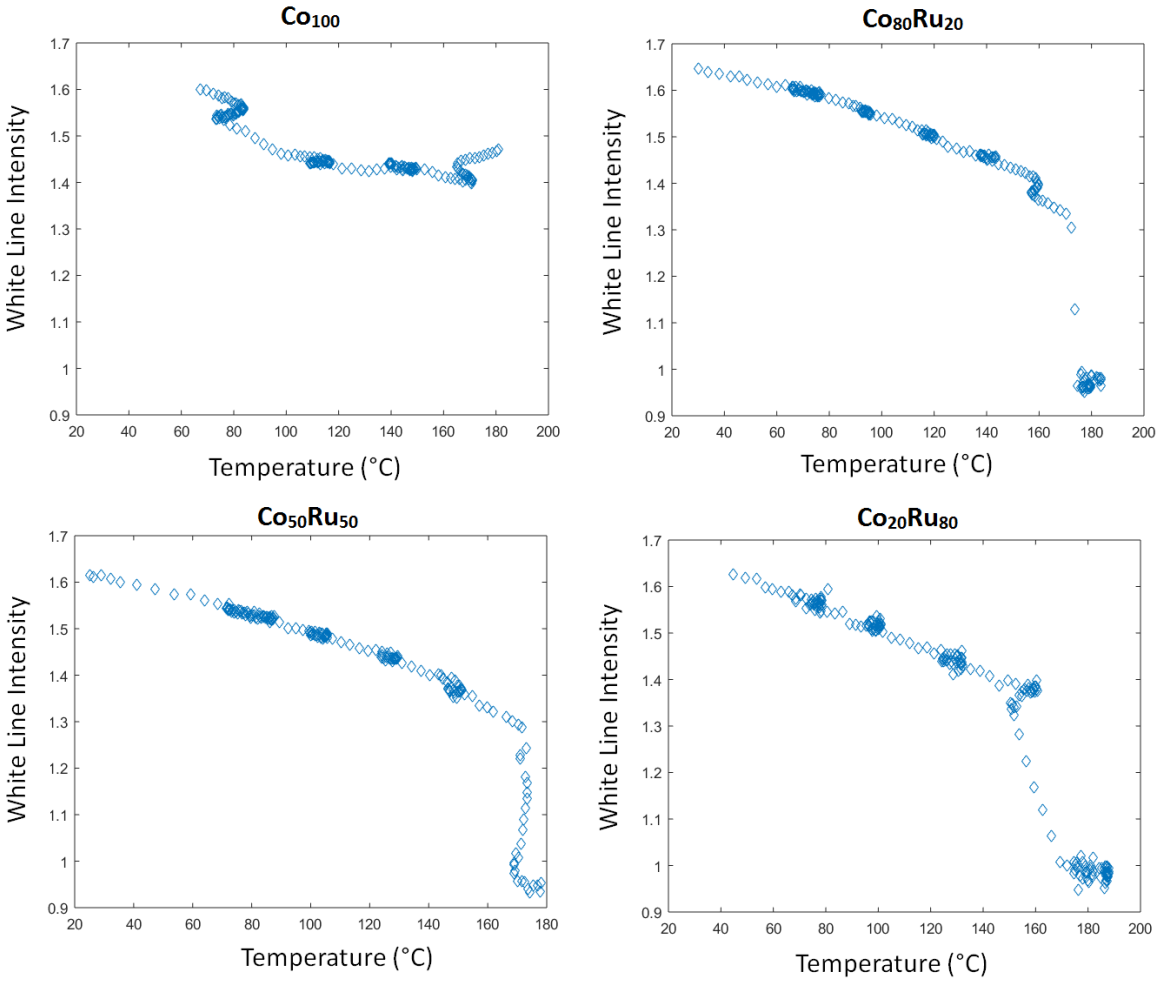

Figure S13. Evolution of the white line intensity during the heating of the precursor solutions having different Co_xRu_{100-x} compositions.

The reduction behavior of Co(II) in octan-1-ol depends on the presence, or not, of Ru(III) cations. Figure S13 is related to the reduction of Co(II) in solutions containing no Ru(III). In this figure, the XAS spectrum at the Co K-edge of a solution of $Co(acac)_2$ in octan-1-ol after the *in situ* experiment (including heating to the boiling point, a stage for *ca.* 15 min and cooling) is compared to spectra related to Co(0) and CoO references. It clearly shows that it is similar to CoO and that a longer heating duration is necessary to induce the reduction to Co(0).

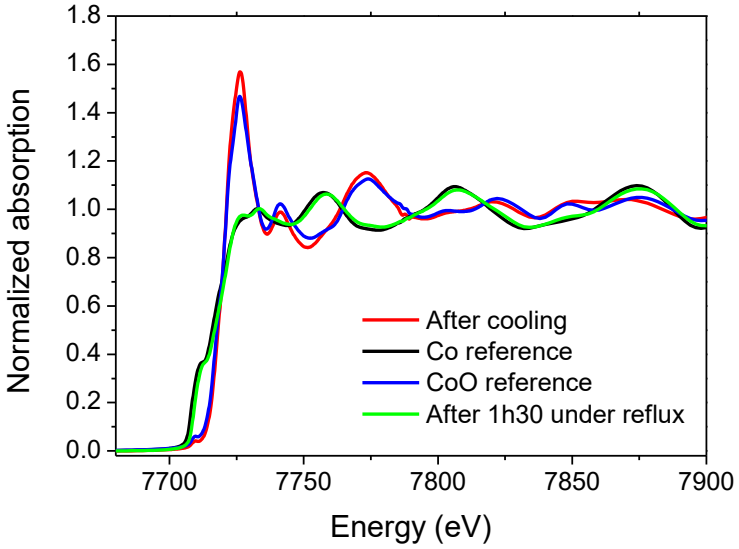

Figure S13. XAS spectra at the Co K-edge of the solution containing $Co(acac)_2$ in octan-1-ol after cooling (in red) compared to Co(0) (in black) and CoO (in blue) references. The spectrum in green corresponds to the $Co(acac)_2$ solution in octan-1-ol heated under reflux for 1h30.

The PCA method allowed to determine that 3 different species are present during heating a solution of $Co(acac)_2$ in octan-1-ol. The spectra of the 3 components were isolated from the experience matrix by MCR-ALS (see Figure S14 and Table S3). Their EXAFS spectra are given in Figure S15. The spectrum of species 1 is close to that of the Co acetylacetonate precursor. The EXAFS Fourier Transformed moduli of species 2 shows a small contraction of the distance between Co and O in the first shell of coordination is observed as can be seen in Figure S15.b, from a mean distance of 2.04 ± 0.01 to 1.95 ± 0.01 Å. This can be accounted for the replacement of acetylacetonate ligands by the solvent or by the formation of polymeric Co(II) acetylacetonate species. Species 3 is very close to CoO as discussed in the main text. Figure S16 gives the fit obtained for the Co K edge EXAFS of the $Co_{80}Ru_{20}$ powder obtained *ex situ*.

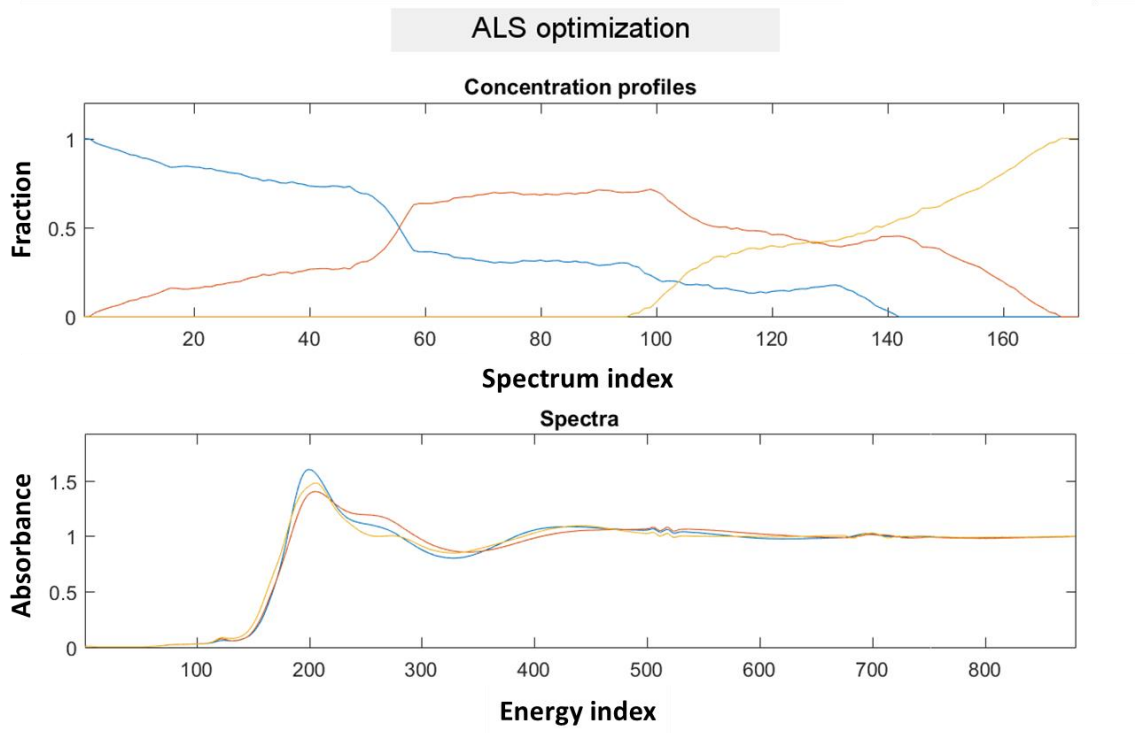

Figure S14. Results of the minimization by MCR-ALS of the Co K edge data set obtained during heating of the Co composition. Constraints used for the minimization were: i) non-negativity of concentrations and absorbance in the spectra, ii) closure of concentrations and iii) unimodality of concentration profiles.

Table S3. Quality factor of the MCR-ALS analysis of the Co K edge XAS data (between 7550 – 8350 eV)

MCR-ALS Quality Indicator as defined in ref. [5]	Value
Standard Deviation of residual *vs*. experimental data	0.0056143
Fitting error (lack of fit) in (%) of experimental data	0.60567
Percentage of variance explained at the optimum	99.9963

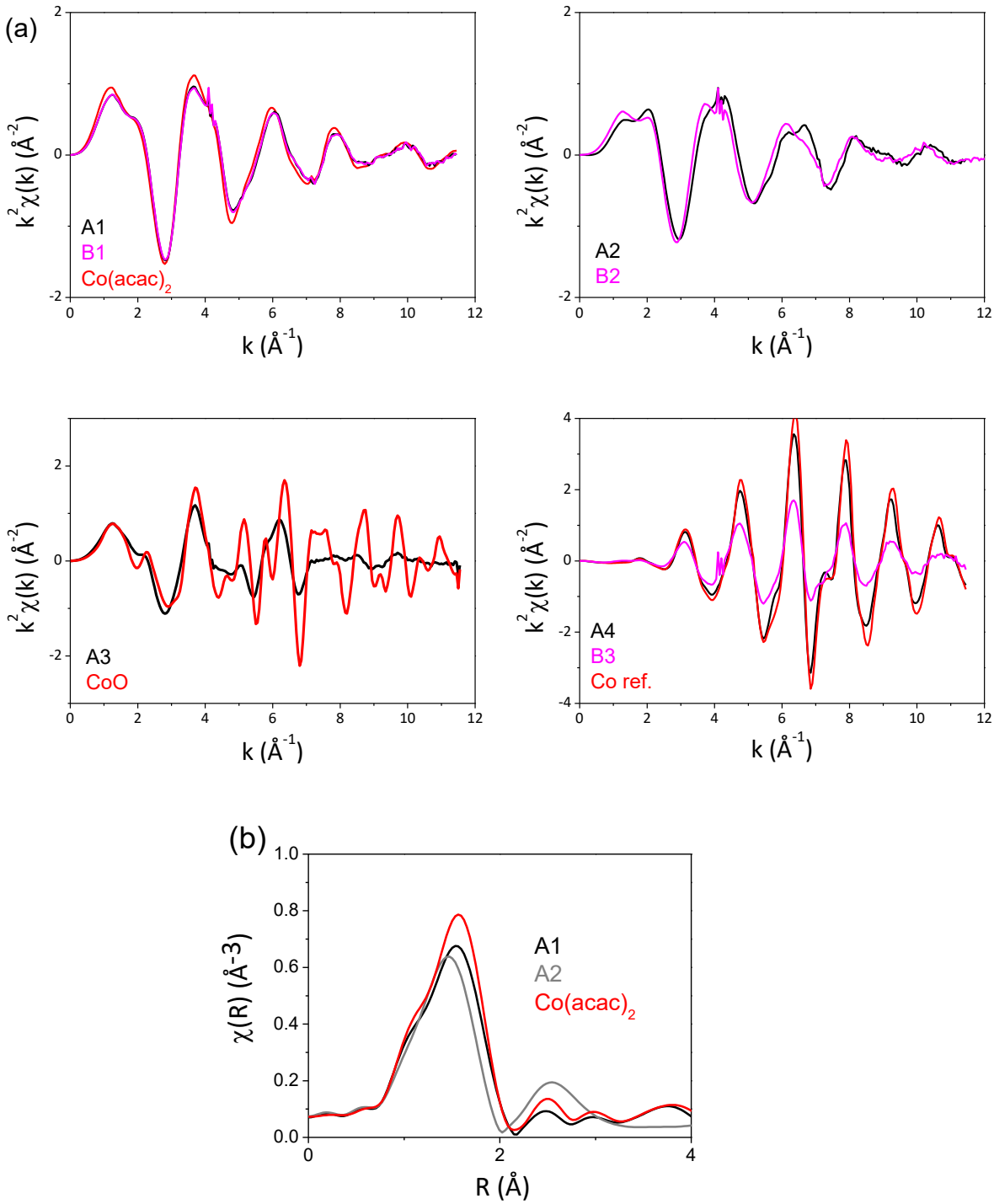

Figure S15. a) k^2 weighted Co K EXAFS of the A1-A3 and B1-B3 (*vide infra*) species formed during heating of a Co or $Co_{80}Ru_{20}$ solution, respectively and of the Co recovered powder after 1h30 at 90 °C (A4) compared to references and b) corresponding EXAFS Fourier transformed moduli of species A1, A2 compared to $Co(acac)_2$.

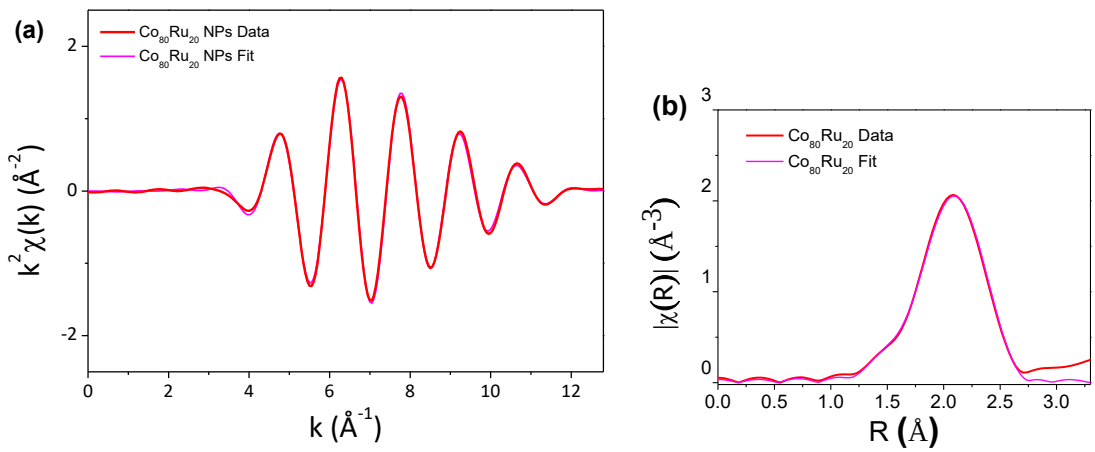

Figure S16. a) Data and fit of a) k^2 weighted Co K EXAFS and b) corresponding EXAFS Fourier transformed moduli for the $Co_{80}Ru_{20}$ NPs. The fits were made between R= 1 and 3 Å; from k = 4.4 to 10.8 with dk = 2 (Kaiser Bessel).

Table S4. Quality factor of the MCR-ALS analysis of the Co K edge XAS data (between 7550 – 8350 eV)

MCR-ALS Quality Indicator as defined in ref. [5]	Value
Standard Deviation of residual *vs*. experimental data	0.0039179
Fitting error (lack of fit) in (%) of experimental data	0.42474
Percentage of variance explained at the optimum	99.9982

The same method was applied for each composition other than Co. Irrespective of the Ru loading, the PCA indicates that three species are also necessary to explain the variance of the data set recorded upon heating (see figure S17). The spectra obtained for all the compositions containing Ru are similar. They are compared to that obtained for pure Co in Figure S15. The initial species is similar but the third one is very different: it is close to CoO for pure Co as discussed previously but corresponds to Co(0) in the presence of Ru. The evolution of each species for the 3 mixed solution is given in Figure S17.

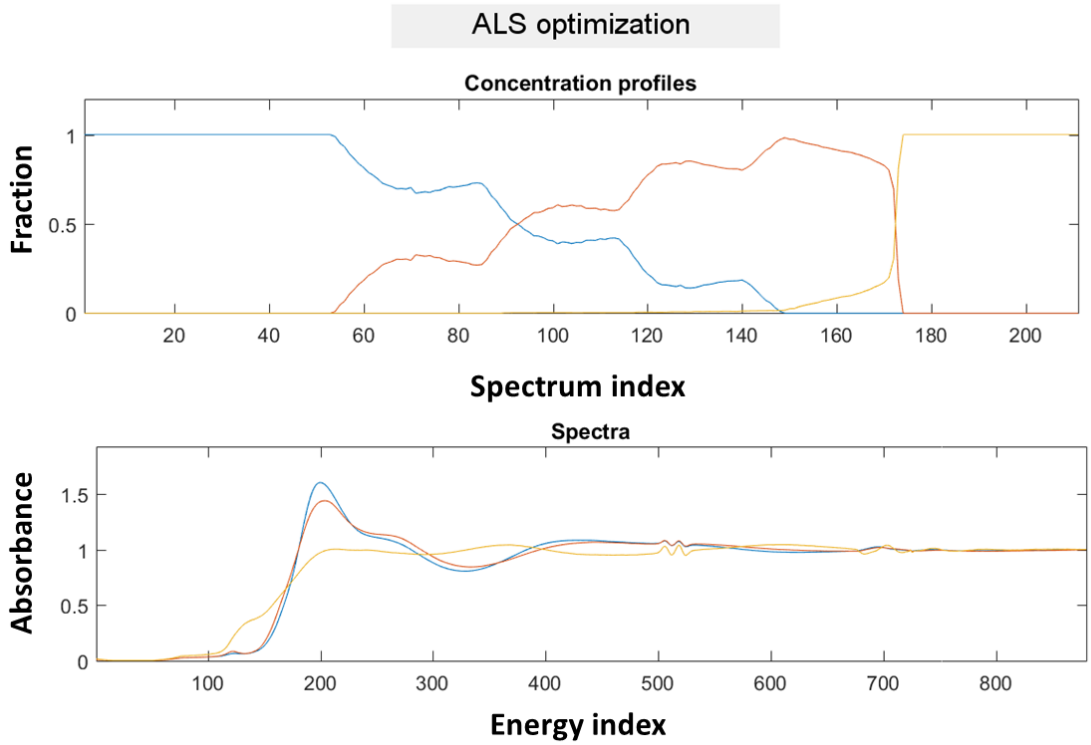

Figure S17. Results of the minimization by MCR-ALS of the Co K edge data set obtained during heating of the $Co_{80}Ru_{20}$ composition. Constraints used for the minimization were: i) non-negativity of concentrations and absorbance in the spectra, ii) closure of concentrations and iii) unimodality of concentration profiles.

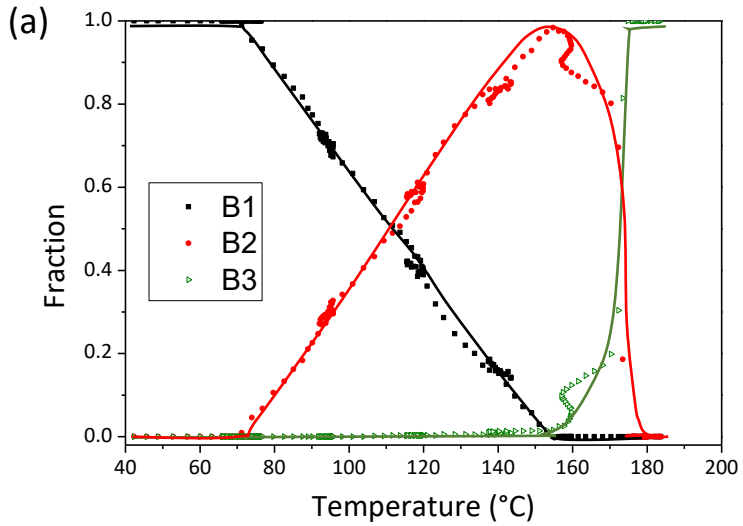

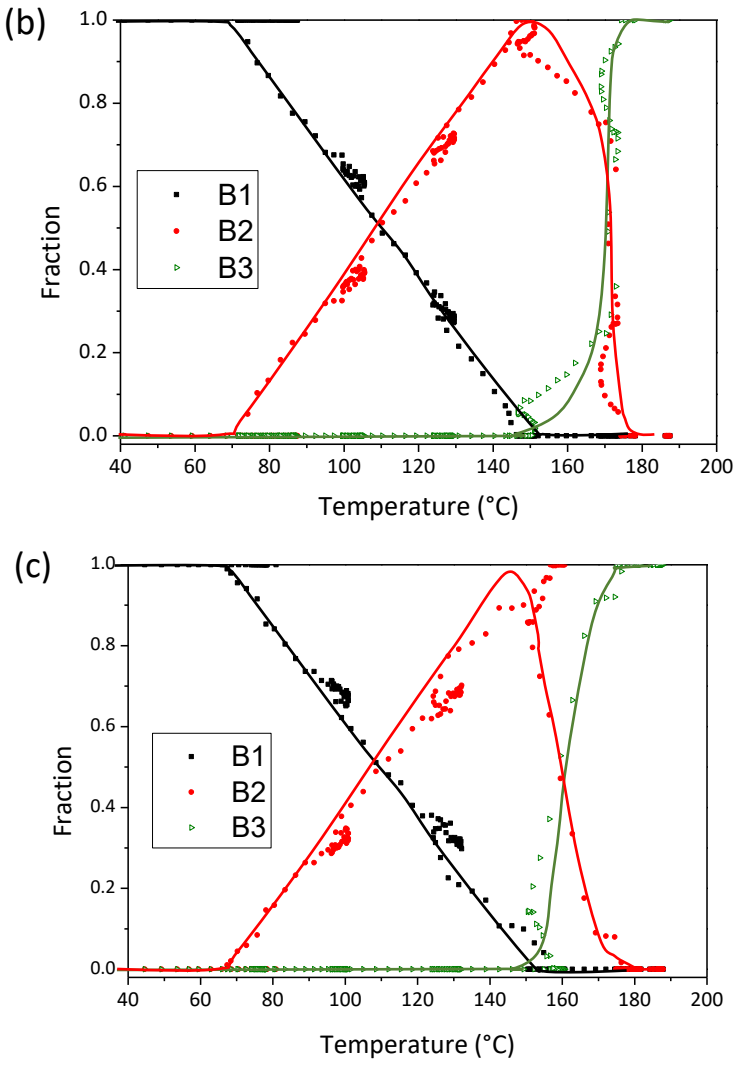

Figure S18. Speciation diagrams for Co as a function of temperature for metal precursor solutions with the composition: a) $Co_{80}Ru_{20}$, b) $Co_{50}Ru_{50}$ and c) $Co_{20}Ru_{80}$ NPs. The points are experimental data and the lines are a guide for the eye giving the tendency.

S3. SAXS studies

UV-visible and X-ray absorption spectroscopies allowed us to follow the reduction of metal cations. Complementary SAXS experiments were performed on aliquots extracted from the reactive Co, Ru and $Co_{50}Ru_{50}$ media at different temperatures to follow the solid formation and obtain morphological information on the precipitated nanoparticles. Figure S19 gives the SAXS diagrams obtained for the Ru, Co and $Co_{50}Ru_{50}$ precursor solutions during heating.

For solutions collected at 60 °C, the signal is nearly flat for Ru solutions indicating the absence of nanoparticles. At 170 °C, only a very small signal is visible, indicating a very small amount of Ru NPs.

The Co and $Co_{50}Ru_{50}$ solutions display a scattering signal at low q even at 60 °C which can be related to non dissolved or polymeric Co acetylacetonate species.

Beyond 180 °C, the intensity increases for all the compositions, which is a clue of the precipitation of the solid. This observation agrees well with the previous results showing a quick reduction at this temperature of Ru and the transformation of Co(II) precursor into CoO for pure Co and Co(0) for the alloys. The slope at low q indicates the presence of big particles (more than 60 nm of radius) or aggregates of thinner ones for all the compositions, which leads the particles to settle out in the flask as the reaction proceeds, also explaining why it was not possible to carry out the characterization of the Co solution during the stage at the boiling stage. For the $Co_{50}Ru_{50}$ solution, the formation of NPs arises 1 minute after the boiling temperature was reached; the peak appearing 4 minutes later is due to nanoparticles interactions.

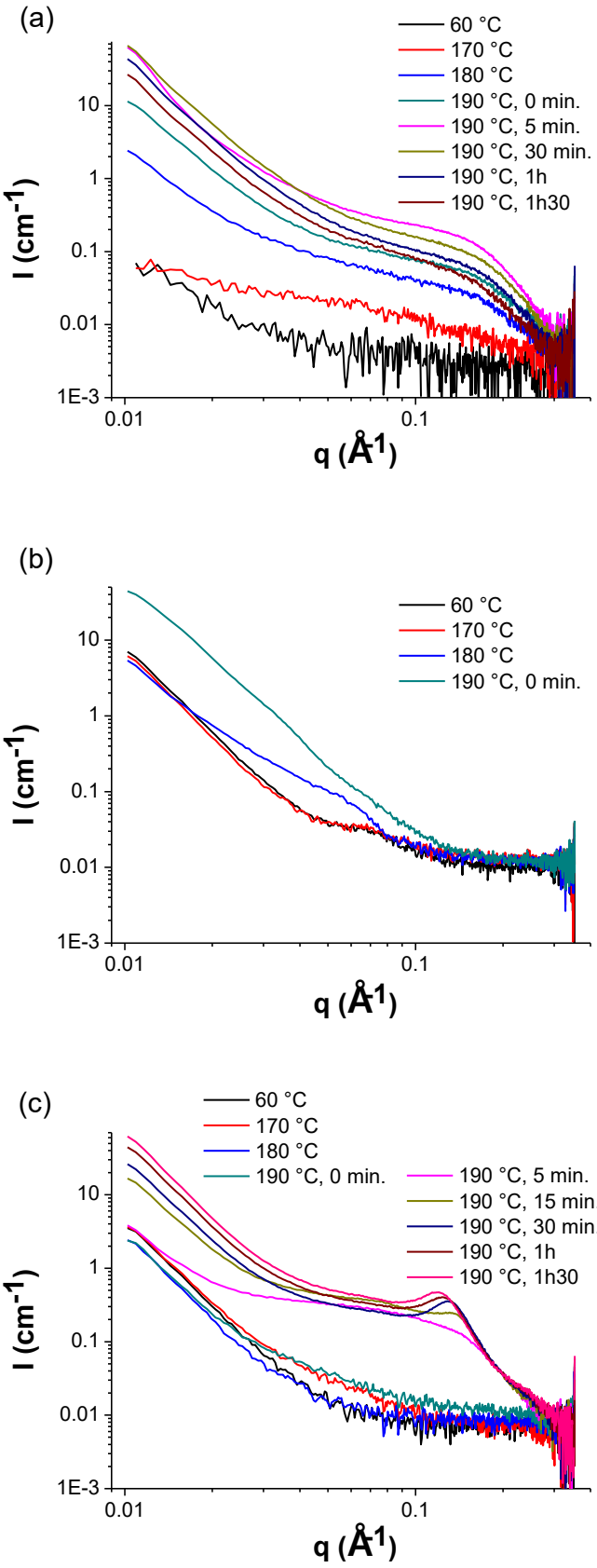

Figure S19. SAXS diagrams recorded on aliquots of reactive a) Ru, b) Co and c) $Co_{50}Ru_{50}$ solutions during heating.

The fraction of solid was deduced from the Invariant theorem and is plotted in Figure S20. The first part of the curve shows a quick increase of solid yield from 160 °C to the boiling point for all the compositions. Notably, the maximum yield of solid, 57 %, was obtained for $Co_{50}Ru_{50}$. The yield decreases for Ru after reaching the boiling temperature (34 %) while no particle could be collected for Co at this point. This is due to the formation of large particles (for Co) or aggregates (for Ru and in a lesser extent for $Co_{50}Ru_{50}$) which settle down in the flask. Consequently, the yields given by SAXS on aliquots are not representative of the global precipitation yield and permits to determine the temperature at which the solid begins to precipitate.

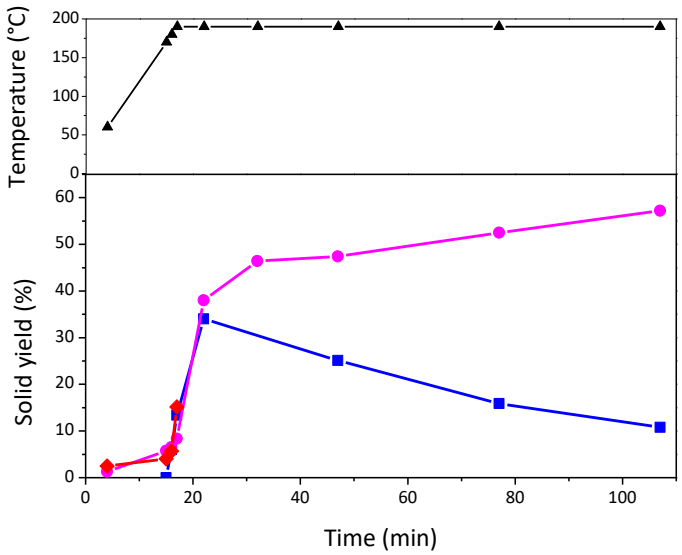

Figure S20. Temporal evolutions of the yield of solid during heating the precursor solutions of Ru (■), $Co_{50}Ru_{50}$ (●) and Co (◆); the temperature profile (▲) is also plotted.

The data were further fitted using Sasview software as displayed in Figure S21.

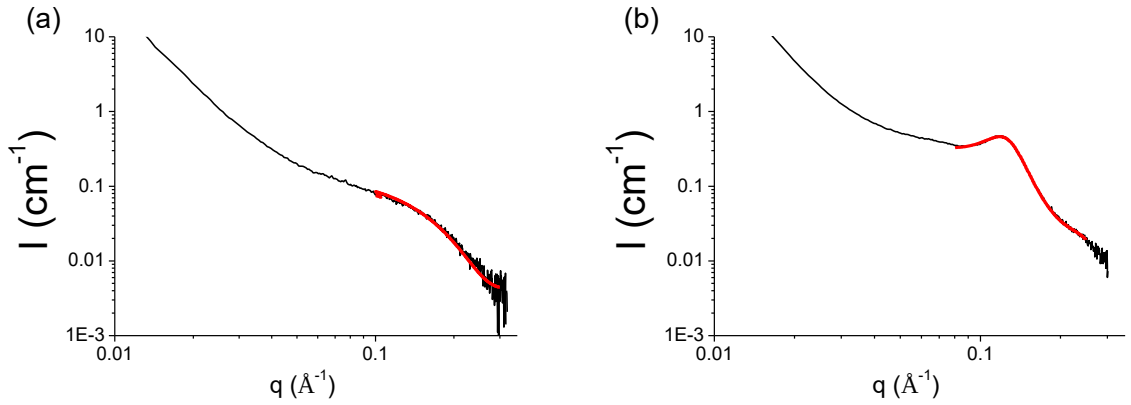

Figure S21. Fit (red curve) of the SAXS diagram (black curve) of a) the Ru precursor solution and b) the $Co_{50}Ru_{50}$ precursor solution after 1h30 heating at the boiling point.

The SAXS curves for the Ru solutions were fitted using a model of polydisperse spheres, giving a radius increasing from 9.3 nm (polydispersity of 1.46 %) at 170 °C to *ca.* 13 nm (polydispersity of 0.08 to 0.38 %) during the stage at the boiling temperature (see Figure S21). The curves for the $Co_{50}Ru_{50}$ composition were also fitted. The best fits were obtained using a cylinder model. They were well fitted with a diameter of 5.4 nm (a little more than the diameter of 3.9 nm deduced from TEM), a polydispersity of 0.4, and a thickness of 1.6 nm. As the reaction proceeds, a correlation peak appears after 30 min at the boiling point, corresponding to a distance of *ca.* 4.8 nm. This is due to an interaction between the nanoparticles probably sticking side to side, and subsequently resulting in their sedimentation.

S4. Gas chromatography analysis

Figure S22 gives the chromatographs of the gas evolved during the synthesis (a) and of the liquid phase recovered after the synthesis of the $Co_{80}Ru_{20}$ sample (b). Pure hydrogen was found to be produced during reduction of the metal salts through dehydrogenation of the octan-1-ol. In the liquid phase, several products were detected (acids, esters , alkenes, …), octanal being the main one (*ca.* 7 mol. %).

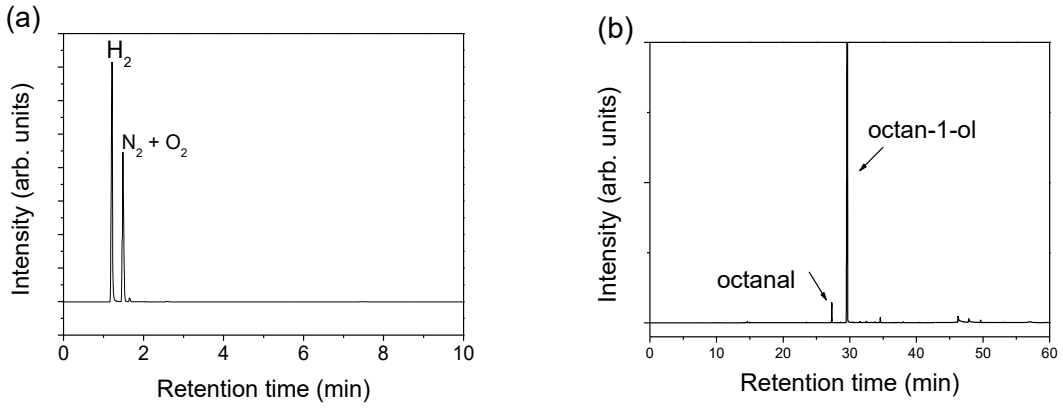

Figure S22. Gas chromatograms of the gas phase after 1 h of reaction (a) and of the liquid phase recovered after the synthesis of the $Co_{80}Ru_{20}$ sample (b).

References

1 M. A. Bennett, M. J. Byrnes and A. C. Willis, Bis(acetylacetonato)ruthenium(ii) complexes containing alkynyldiphenylphosphines. Formation and redox behaviour of [Ru(acac)2(Ph2PC≡CR)2] (R = H, Me, Ph) complexes and the binuclear complex cis-[(Ru(acac)2)2(μ-Ph2PC≡CPPh2))2], *Dalt. Trans.*, 2007, **2**, 1677–1686.

2 S. Duman, M. Masjedi and S. Özkar, Highly active and long lived homogeneous catalyst for the dehydrogenation of dimethylamine borane starting with ruthenium(III) acetylacetonate and oleylamine precatalyst, *J. Mol. Catal. A Chem.*, 2016, **411**, 9–18.

3 P. A. Reynolds, J. W. Cable, A. N. Sobolev and B. N. Figgis, Structure, covalence and spin polarisation in tris(acetylacetonato)ruthenium(III) studied by X-ray and polarised neutron diffraction †, *J. Chem. Soc. Dalt. Trans.*, 1998, 559–570.

4 R. B. Cattell, The Scree Test For The Number Of Factors, *Multivariate Behav. Res.*, 1966, **1**, 245–276.

5 J. Jaumot, A. de Juan and R. Tauler, MCR-ALS GUI 2.0: New features and applications, *Chemom. Intell. Lab. Syst.*, 2015, **140**, 1–12.